In Situ Optical Studies of Solid-Oxide Fuel Cells

Michael B. Pomfret,[1] Jeffrey C. Owrutsky,[1] and Robert A. Walker[2]

[1]Chemistry Division, Naval Research Laboratory, Washington, District of Columbia 20375

[2]Department of Chemistry and Biochemistry, Montana State University, Bozeman, Montana 59717; email: rawalker@chemistry.montana.edu

Annu. Rev. Anal. Chem. 2010. 3:151–74

First published online as a Review in Advance on March 1, 2010

The *Annual Review of Analytical Chemistry* is online at anchem.annualreviews.org

This article's doi: 10.1146/annurev.anchem.111808.073641

1936-1327/10/0719-0151$20.00

Key Words

spectroscopy, thermal imaging, infrared, Raman

Abstract

Thermal imaging and vibrational spectroscopy have become important tools for examining the physical and chemical changes that occur in real time in solid-oxide fuel cells (SOFCs). Imaging techniques can resolve temperature differences as fine as 0.1°C across a SOFC electrode at temperatures higher than 600°C. Vibrational spectroscopy can identify molecular species and changes in material phases in operating SOFCs. This review discusses the benefits and challenges associated with directly observing processes that are important to SOFC performance and durability. In situ optical methods can provide direct insight into reaction mechanisms that can be inferred only indirectly from electrochemical measurements such as voltammetry and electrochemical impedance spectroscopy and from kinetic models and postmortem, ex situ examinations of SOFC components. Particular attention is devoted to recent advances that, hopefully, will spur the development of new generations of efficient, versatile energy-producing devices.

1. OVERVIEW

1.1. Background

Ever since the first fuel cell was described ~170 years ago, such devices have been studied extensively as potential sources of electrical power (1, 2). Several properties of fuel cells make them attractive alternatives to conventional combustion sources. Because fuel cells produce energy directly from electrochemical oxidation, they are both cleaner and more efficient than internal combustion engines (3). Furthermore, fuel cells have no moving parts, which simplifies their maintenance and scaling. Consequently, fuel cells are suitable for both portable and stationary applications as well as for auxiliary power units (2–5). Of the different types of fuel cells that convert fuel and oxygen directly into electricity and products, the solid-oxide fuel cell (SOFC) stands out by virtue of its ability to (*a*) convert fuel into electricity with a theoretical efficiency approaching 75% and (*b*) use a wide variety of fuels including H_2, syngas, and higher-molecular-weight hydrocarbons (6).

SOFCs are currently being developed for commercial applications that require power outputs in the 1–100-kW range (3, 7). These cells also require high operating temperatures due to the large energetic barriers for O_2 dissociation at the cathode and the ~100–kJ mol^{-1} activation energy associated with oxide-ion diffusion through the SOFC electrolyte (8). Although high-temperature operation introduces challenges in terms of device construction and cell durability, it also reduces the susceptibility of SOFCs to poisoning and permits the use of complex fuels (9). Because of their high temperatures, SOFCs are suitable for applications that use readily available excess heat and are one of the few types of fuel cells that can operate with hydrocarbon fuels and fuel mixtures (10). For example, SOFCs have been integrated into the exhaust streams of conventional, coal-fired power plants to convert unused fuel in the effluent into additional power (11). SOFCs are also well suited to local, small-scale applications that require quiet operation and ease of deployment. Expanding the use of SOFCs requires improving cell efficiency and longevity, two factors that are affected by specific details of the gas-phase fuel mixture as well as by the susceptibility of cell materials to potential contaminants at the electrodes. Consequently, most current fuel cell research focuses on resolving these two issues (4, 6, 12).

Electrochemical measurements and kinetic models have proven effective at predicting how SOFC performance will respond to changes in operating conditions (13–21), and extensive ex situ studies of SOFC components carried out after operation have shown how electrode and electrolyte microstructures evolve (10, 22, 23). These approaches, however, fail to provide real-time diagnostics and lack the molecular specificity necessary to distinguish various physical and chemical processes in operating cells. A new focus of SOFC research employs both in situ optical techniques, including thermal imaging and vibrational spectroscopy, to characterize the chemistry occurring in SOFCs and electrochemical measurements that quantify device performance (24–28). Data from these combined approaches provide new, detailed information that can be used to validate and improve kinetic models; correlate molecular species observed directly with electrochemical performance; and address fundamental questions about how SOFCs operate and why they fail.

1.2. Solid-Oxide Fuel Cell Components

A schematic representation of a SOFC membrane electrode assembly (MEA) is shown in **Figure 1**. The standard electrolyte material is yttria-stabilized zirconia (YSZ), although other materials are being developed to improve cell performance and durability (8, 29–35). The 8–10-mol%

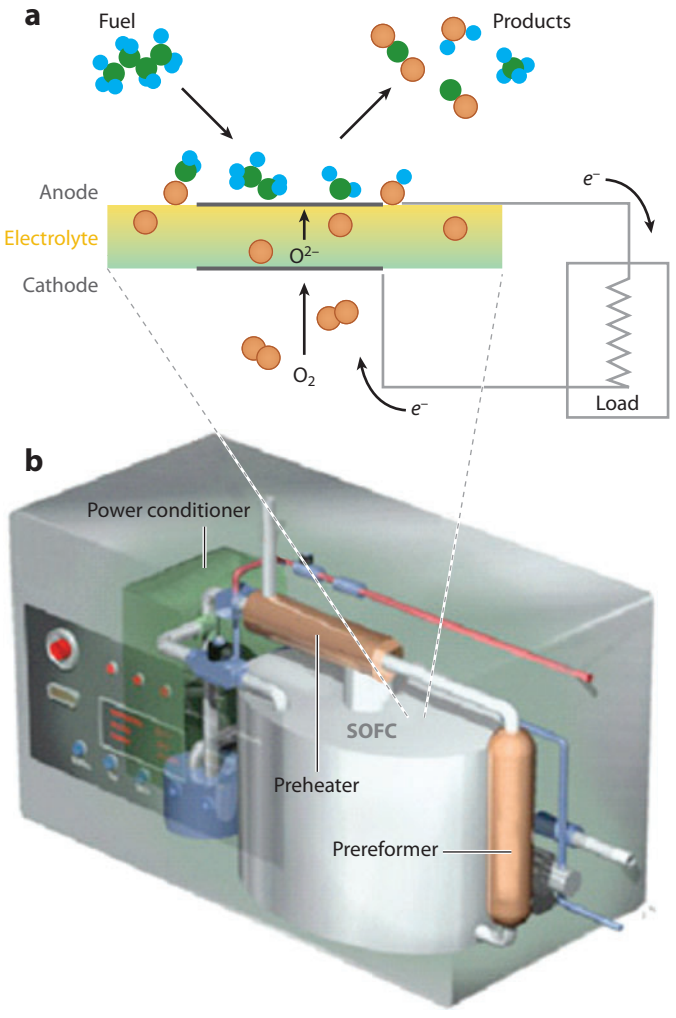

Figure 1

(*a*) Schematic diagram of a solid-oxide fuel cell (SOFC). Its primary components and their principle functions are indicated. Oxygen molecules are reduced at the cathode to form oxide ions that are transported through the solid electrolyte to the anode, where they oxidize fuel. Electrons from the fuel are conducted through a load to complete the circuit. (*b*) Diagram of a commercial SOFC stack. Image taken from **http://www.netl.doe.gov/publications/TechNews/tn_ge_benchmark.html**.

yttria dopant creates oxide vacancies in a stable cubic zirconia lattice, thus allowing for oxide-ion conduction at temperatures above 600°C (2). Cathodes, wherein molecular oxygen is reduced catalytically to form oxide ions, typically consist of perovskite oxides such as lanthanum strontium manganite (LSM), although fine Pt mesh has also been used (36–44). Fuel oxidation and electricity production occur at the anode, which is commonly a porous nickel/YSZ cermet material (2). Numerous other anode materials have been proposed for use in SOFCs (4, 12, 45–60). For example, ceria and copper have been shown to be less susceptible to poisoning from graphite deposition (9).

2. BACKGROUND AND JUSTIFICATION FOR OPTICAL INVESTIGATION

2.1. Issues Concerning Solid-Oxide Fuel Cell Operation

Although SOFCs are widely studied and are currently in advanced commercial development, there continue to be concerns regarding the efficiency and durability of these devices. With typical devices functioning at temperatures higher than 700°C, the kinetics of any process that leads to material degradation and/or transformation happen much more quickly than at lower temperatures, from where most of the empirical data used for predictive modeling arise. Also, the precise mechanisms responsible for fuel oxidation remain mostly speculative because analytical techniques capable of determining the molecular-level chemistry occurring in operating SOFCs are still being developed. Traditional electrochemical methods, such as electrochemical impedance spectroscopy (EIS) and voltammetry, can report on macroscopic electrochemical behavior (14–18, 21) but cannot identify the specific reaction pathways responsible for fuel oxidation or oxygen reduction.

An advantage of SOFCs is their ability to utilize various fuels, but this feature also results in more complex anode chemistry that can be challenging to quantify. For example, a mechanism proposed to describe SOFC chemistry is direct electrochemical oxidation (DECO) (57, 61–64). A balanced DECO reaction with methane as a fuel is

$$CH_4 + 2O_2 \rightarrow CO_2 + 2H_2O.$$

In reality, multiple reaction pathways, including the formation of side products from incomplete oxidation as well as nonelectrochemical processes such as reforming and pyrolysis (9, 12, 61, 65–69), are available to the reactants. For example, hydrocarbons react with steam under reforming conditions to form molecular hydrogen and CO. These species can then participate more efficiently in electrochemical oxidation at the anode, thus reducing the likelihood of carbon deposits (70–72). Consequently, in a SOFC operating with a methane feed, the actual fuel participating in electrochemical oxidation can be CH_4, CO, H_2, or any larger hydrocarbon that may form as a result of gas-phase reactions.

Pyrolysis and reforming of higher-molecular-weight, carbon-containing fuels pose distinct challenges to the development of kinetic models describing SOFC chemistry because these processes change the composition—and the resulting reactivity—of the incident fuel mixture (64, 69–74). Due to pyrolysis, a predictive mechanism of cell performance cannot focus on the electrochemical oxidation of the parent fuel alone. Butane, for example, forms a mixture of ethylene, methane, and propylene at temperatures above ~650°C (75). Each of these fuels displays distinctive electrochemical behavior and different propensities to either oxidize or form carbon deposits. Furthermore, pyrolysis and reforming affect the product yields so that they depend not only on the fuel used but also on the conditions of the fuel inlet (e.g., temperature and residence time) (69–74). Therefore, an interpretation of electrochemical oxidation in SOFCs must begin before the reactants reach the anode. If industrial fuels or fuels derived from biomass are to be used, sulfur contaminants such as H_2S become a concern (76–78). Poisoning of Ni anodes both by carbon and by sulfur reduces cell efficiency, presumably by blocking electrocatalyst sites. Gas-phase sulfur promotes the formation of new nickel sulfide materials that are inert and insulating (6), but in the absence of direct, in situ, molecularly specific data, other mechanisms proposed to be responsible for SOFC degradation remain speculative.

2.2. Conventional Experimental Techniques

High operating temperatures require that SOFC architectures be self-contained and well insulated in order to minimize thermal losses to the surroundings. As a result, traditional SOFC devices preclude experimental studies by any diagnostic approach requiring direct visual observation. The most common in situ techniques used to examine SOFC chemistry have been electrochemical methods such as linear sweep voltammetry and EIS (14–18, 21). These techniques have proven very effective at demonstrating that SOFC performance depends on fuel composition, temperature, electrode microstructure, and overpotential; however, electrochemical data cannot provide direct information about the mechanisms responsible for converting O_2 and fuel into electricity and products, nor can these methods directly identify the properties responsible for changes in performance on the component level.

Almost every new advance in SOFC development is accompanied by electrochemical studies showing that new materials or new geometries improve SOFC performance. Figures of merit often include increased power densities, reduced impedances, and/or improved device durability. These data are then used to construct models that have predictive capabilities and, hopefully, mechanistic insights. Although these models can be very versatile and instructive in terms of forecasting how SOFC performance will depend on conditions and cell geometries, the models themselves are based on properties that are difficult to measure directly (13, 19, 20). Model input extrapolated from room-temperature studies or from experiments carried out under different conditions (e.g., ultrahigh vacuum) include transport properties (such as gas-phase and surface-diffusion coefficients), sticking probabilities, and activation energies (79–94). Often, these models are verified indirectly by correlating experimental electrochemical data with controlled changes in cell operating conditions.

A second strategy used to deduce the chemistry occurring in SOFCs is to carry out extensive ex situ analyses following SOFC operation under well-defined conditions. Once a cell has been cooled back to room temperature and disassembled, a variety of analytical tools can be used to exhaustively characterize the "postmortem" condition of various SOFC components. Multiple analytical techniques have been used to study cells, including mass spectrometry (MS), X-ray photoelectron spectroscopy (XPS), X-ray diffraction (XRD), and X-ray absorption spectroscopy (XAFS) (76, 95–98). Examples of such studies include the examination of SOFC cathodes with XRD (99), MS–gas chromatography analyses of carbon deposits left behind by unreacted hydrocarbon fuels (9), and analyses of changes in cell structure due to aging from long-term use (23). Cell-exhaust species can be identified via MS and Fourier transform infrared spectroscopy (FTIR), but these techniques do not necessarily provide specific information about the species present at the MEA (98, 100). Although findings from these studies can be informative, conclusions from ex situ measurements must be tempered by acknowledging that results can be affected by chemistry occurring as the SOFC cools.

When constructing kinetic models, one generally assumes that quantities, be they calculated, inferred indirectly, or measured ex situ, are accurate despite the high temperatures and the electrochemically complex environments found at SOFC electrodes. To test different proposed models of oxygen reduction and fuel oxidation, spectroscopic experiments must be able to identify specific intermediates of reduction/oxidation processes, determine where these intermediates form, and explain how the presence of these intermediates depends on cell operating potentials and fuel composition. Furthermore, in situ spectroscopic experiments should be able to correlate physical and materials changes, such as phase transitions and changes in composition, with variations in SOFC performance measured by voltammetry and EIS. A list of techniques and their applications to SOFC systems is given in **Table 1**.

Table 1 Survey of experimental methods to characterize solid-oxide fuel cells[a]

Technique	In situ or ex situ	Observable(s)	Strength(s)	Weakness(es)
Electrochemical voltammetry	In situ	Current and power density	Ultimate performance metric	Often chemically ambiguous and model specific
Impedance spectroscopy	In situ	Cell and electrolyte resistance	Activation barriers and ohmic losses	Often chemically ambiguous and model specific
Products				
Mass spectroscopy	Ex situ	Gas products and fuel utilization	Monitors efficiency	Indirect, vulnerable to interferences
XPS	Both	Material composition and structure	Material specific	Challenging in situ, elemental rather than molecular information
EXAFS	In situ	Composition and adsorbates	Chemically specific	Challenging for experiments and interpretation
Optical				
Raman spectroscopy	In situ	Composition, structure, and temperature of materials and adsorbates	Molecular and material specific, kinetics, real time	Used for a single position at a time
Infrared spectroscopy	In situ	Surface species	Adsorbate structure specific, broad spatial coverage, real time	Experimentally challenging
Imaging	In situ	Emission, temperature	Spatially resolved, real time	Lacks molecular specificity

[a]Abbreviations: EXAFS, extended X-ray absorption fine structure; XPS, X-ray photoelectron spectroscopy.

2.3. Implementing Optical Techniques

Most analytical techniques require conditions that are not well suited for SOFC operation. For example, both XPS and XAFS have been used in situ, but their use required half-cell configurations and pressures that were much lower than those typically found in operational cells (76, 101). There is considerable interest in the development of nondestructive, robust, easily implemented in situ optical diagnostics capable of directly characterizing the physical properties—such as temperature, structure (thermally induced stress), and composition—of SOFC components. To employ different optical methods in the study of SOFC chemistry, one must modify fuel cell devices to allow for optical access while preserving the fuel cell performance. This requirement creates engineering concerns including, but not limited to, heat loss, thermal gradients, and fuel-flow dynamics. From an experimental perspective, collection optics must be protected from overheating, cracking, burning, and melting.

Recent work employing a variety of approaches has overcome these and other obstacles. Although these approaches are still not routine, advances made during the past several years have shown that different optical methods can provide the information necessary to revisit and refine proposed models of SOFC chemistry. Thermal imaging has long been used to investigate high-temperature systems, and it has also recently been used in studies of proton-exchange membrane fuel cell systems (102–105). Spectroscopic measurements of SOFC-relevant materials, such as YSZ and carbon species, have been made at high temperatures (106–108). Recently, work has been published on thermal imaging as applied to SOFC systems, taking advantage of the black-body radiation associated with SOFC temperatures. IR and Raman spectroscopies have identified chemical reaction intermediates as well as poisons on SOFC surfaces, and thermal

imaging has been used to determine the effect of various chemical and electrochemical processes on the temperature of the cell surface (24–26, 28, 69, 77, 109–111).

3. IN SITU IMAGING OF SOLID-OXIDE FUEL CELL ELECTRODES

3.1. Imaging Background

Optical diagnostics have been developed and applied to a number of areas in energy science (broadly defined), including combustion and flames (112–117); fire detection (118); and nondestructive thermography of high-temperature solids (119), such as ceramics and thermal barrier coatings (120). For example, optical techniques have been used in combustion and flame studies to monitor conditions such as temperature and pressure and to characterize the relevant transport and kinetics resolved in both space and time. These properties are also relevant to processes that occur in SOFCs.

One of the main challenges in SOFC development is reducing thermal stress and gradients induced by oxidation and reforming. Temperature stability is an important SOFC design principle that governs the sensitivity of different architectures to the thermal expansion coefficients of the different materials and components. Sudden changes in operational temperature can lead to MEA failure (6, 7, 121). Because SOFC models often provide predictions of temperature as a function of operational conditions and location in the cell, experimental temperature measurements can serve as a useful diagnostic to test their accuracy and the range of conditions in which models remain valid (94, 122). Also, contaminants and thermal gradients can undermine performance and induce component or cell failure, so the location and identification of incipient thermal gradients may provide insight into degradation processes. In most cases, temperature monitoring has been carried out on operating cells via thermisters and thermocouples (TCs), which typically monitor only one or a few positions at a time and are invasive, given that they can contaminate electrodes or cause thermal instabilities (123–125).

Another way to monitor temperature is to take advantage of the emitted thermal radiation from the SOFC itself. Thermal imaging is an emerging method that has numerous advantages for characterizing SOFC temperatures. Because the technique is noninvasive and is capable of standoff detection, it is not susceptible to the problems associated with the use of TCs to monitor temperature. Thermal imaging also provides wider spatial coverage, nominally over an entire side of a button cell, with a resolution limited by the optics and camera. In SOFC applications, the biggest challenge—which is common to all in situ optical methods—is the design and construction of a device that provides optical access. With an imaging camera, the appropriate transmitting window material, and a long-pass or narrow-band filter, emission intensity can be measured and used to determine the thermal emission profile in real time over a wide area with high spatial resolution. Thermal imaging of SOFCs was first reported by Brett et al. (24), who employed a narrow-band filter near 4 μm and a mid-infrared (MIR) InSb camera to monitor the emission from SOFC cathodes. More recently, researchers recognized that the high temperatures of SOFCs permit thermal imaging at shorter wavelengths, where optical components and instruments are less expensive and provide better sensitivity with higher spatial resolution. Near-infrared (NIR) thermal imaging with Si-based charge-coupled device (CCD) cameras of high-temperature objects has been reported and analyzed (126, 127); for instance, investigators have developed applications for remote detection of fire (118, 128). At wavelengths corresponding to the long-wave edge of Si detectors (~1 μm), emission can be detected and used to determine the temperature of objects as cold as ~400°C. The sensitivity for thermal detection (which depends on the temperature dependence of the emission) increases with decreasing wavelength; as long as it is possible to

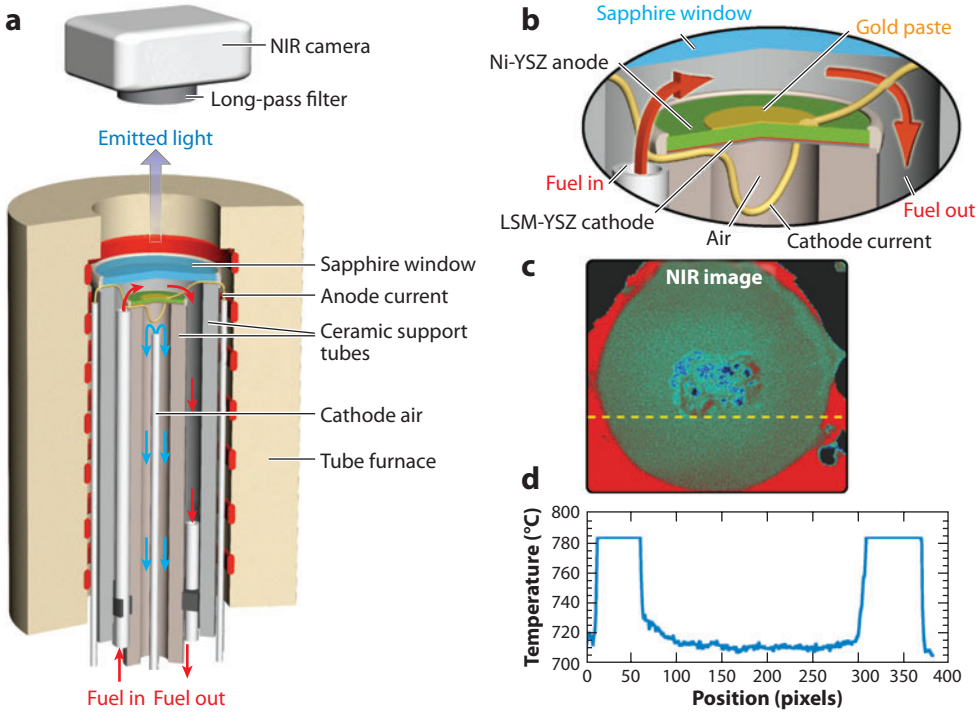

Figure 2

Schematic diagram of (*a*) a solid-oxide fuel cell (SOFC) thermal imaging apparatus, (*b*) an expanded view of the button cell geometry, (*c*) a representative thermal image of an anode-supported SOFC, and (*d*) a horizontal temperature profile (*blue line*). Abbreviations: LSM, lanthanum strontium manganite; NIR, near-infrared; YSZ, yttria-stabilized zirconia. The images in panels *a* and *b* are provided courtesy of Prof. Robert Kee.

observe emission at the lowest temperature of a desired range, the shortest wavelength is the best choice in terms of theoretical sensitivity. There are additional practical advantages to using shorter wavelengths for thermal imaging. Cameras and optical components are less expensive and, in many respects, yield better performance. NIR imaging has been used to monitor anodes of SOFCs operating on hydrogen and hydrocarbon fuels, as described below. A schematic of an in situ NIR imaging apparatus for SOFCs is shown in **Figure 2**.

3.2. Mid-Infrared Thermal Imaging of Solid-Oxide Fuel Cells

The earliest thermal imaging studies on SOFCs were carried out by two groups (24, 25), who monitored MIR emission from cathodes of button cells. Both groups measured temperature profiles across electrode surfaces as the cells were polarized to various voltages. Their results illustrated the high spatial resolution available with this technique and showed that data can be quickly collected and readily correlated to theoretical predictions. Results even provided input used to refine the models themselves.

The first thermal imaging study was published by Brett et al. (24), who demonstrated the effect of polarization on cathodes of gadolinium-doped ceria (GDC)-based button cells. GDC electrolyte

supports were used to promote the activity of cells at lower operating temperatures (500–650°C, compared to 700–900°C when YSZ electrolytes were used). H_2 was used as the fuel over Ni/GDC anodes, while a lanthanum, strontium, cobalt, iron oxide (LSCF) cathode was exposed to ambient air. Radiation in the 4-μm–wavelength range was measured with a liquid nitrogen–cooled InSb camera; a spatial resolution of <1 mm and a temperature resolution of ~0.1°C were achieved (24). This study indicated that the cathode-side surface of the SOFC remained at a constant temperature while the cell was held at open-circuit voltage (OCV). However, when the cell was polarized to 0.2 V, temperature gradients of 1.0 to 1.7°C were observed across the cell (**Figure 3*a*,*b***). The spatial profiles of the temperature changes were ascribed to geometrically inconsistent current densities, contacts between the current collectors and electrodes, electrode deterioration, and variations in the structures of the SOFC components. General aspects of the temperature increases in polarized cells were attributed to cell self-heating caused by electrochemical reactions at the electrodes and by

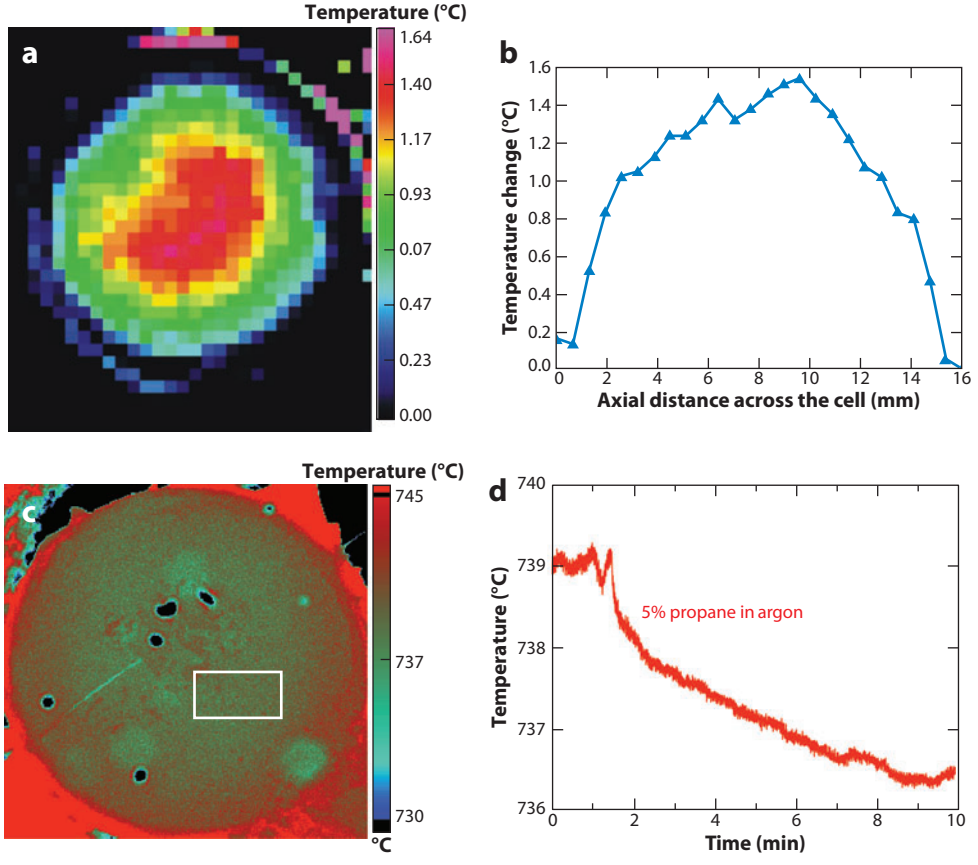

Figure 3

Results from (*a*,*b*) mid-infrared (MIR) and (*c*,*d*) near-infrared (NIR) thermal imaging studies of solid-oxide fuel cells (SOFCs). In both cases the cells are ~2.5 cm in diameter. The MIR imaging studies were carried out on LSCF (lanthanum, strontium, cobalt, iron oxide) cathodes; thermal images (*a*), as well as spatial profiles (*b*), were determined. (*c*) NIR images and (*d*) time series of temperature variations for the area indicated by the white box in panel *c* were reported for Ni/YSZ (yttria-stabilized zirconia) anodes of SOFCs operating on hydrocarbon fuels. Panels *a* and *b* are adapted from Reference 24 with permission. Copyright 2007, Elsevier. Panels *c* and *d* are reproduced from Reference 28 with permission. Copyright 2010, Elsevier.

current flow through the cell. Specifically, the heat was generated by (*a*) the change in the entropy of the electrochemical reactions and (*b*) the potential losses resulting from the ohmic resistances in the cell as a whole and the concentration and activation barriers at the electrodes (24). Thermal data from the imaging study were used in a model to predict how temperature variations need to be considered when analyzing polarization data. The small temperature changes associated with the operation of electrolyte-supported cells had only minimal effects on the current and power densities of the cells; however, cells with thin electrolyte layers were predicted to have greater temperature gradients. The models found that temperature changes must be accounted for when studying cell performance (24). The results were also used to determine heat-transfer coefficients, and they helped to demonstrate the validity of using electrolyte-supported button cells to evaluate SOFC performance.

In a second SOFC thermal imaging study, Ju et al. (25) investigated cells supported by scandium-stabilized zirconia electrolytes with Ni anodes and LSCF cathodes. Thermal images of the cathodes were taken in the wavelength range of 3 to 5 μm with a platinum silicide camera, and the results were compared to a heat-transfer model incorporating ohmic and activation resistances. The results indicated temperature changes (0.9–1.6°C) and polarization (0.5–1.0 A) that were similar to those reported by Brett et al. (24). The model reproduced the observed temperature trends, even though predictions of the absolute temperature changes were 15% too high. The discrepancy was attributed to heat losses due to contact with the cell support structure. Considering the polarization losses arising from various resistances in the cell, the study found that at the low end of the temperature range investigated, the ohmic resistance associated with the ion flux through the electrolyte increased by 75% but that the overall polarization resistance of the cell was increased by a factor of three (25).

3.3. Near-Infrared Thermal Imaging of Solid-Oxide Fuel Cells

Recently, Pomfret et al. (28) exploited NIR thermography as a convenient and effective analytical technique for investigating the effects of anode chemistry in operating SOFCs. Ni/YSZ anode–supported cells with YSZ electrolytes and LSM cathodes, which have previously been characterized in terms of their performance (23), were operated at approximately 740°C with air present at the cathode and either hydrogen or propane flowed over the anode. A Si-CCD camera was fitted with a long-pass filter that, combined with the spectral response of the camera, resulted in an effective broadband pass filter between 720 and 1000 nm. The images collected had a spatial resolution of ~0.1 mm, taking into account the lens and positioning of the camera. Temperature resolution was found to be ~0.1°C.

Thermal imaging studies were performed on the anodes of operating SOFCs to explore how temperature changes and anode structures are affected by different fuels. A typical NIR image of one of the cells is shown in **Figure 3*c***. Several types of measurements were carried out, including the following:

1. Temperature changes were determined for different fuels at OCV.
2. Following exposure to a particular fuel at OCV, the cell was run with hydrogen and polarized.
3. Cells were polarized with only Ar in the fuel feed to determine temperatures across the anode as residual graphite and the electrode material itself (e.g. Ni) were oxidized.

In the first measurement, when hydrogen was introduced (at 750°C), the temperature increased 5–10°C due to heat produced during fuel oxidation processes. When propane was introduced, the temperature decreased by 4.0 ± 0.1°C due to the endothermic hydrocarbon dissociation processes

that offset a small amount of fuel oxidation (**Figure 3*d***) (28). In the second measurement, after operation with a particular fuel, the flow on the anode side was changed to hydrogen, and the cells were polarized. Only a slight temperature increase (1–2°C) was observed when the cell was loaded; the effect was similar to the thermal effects of polarization in the MIR imaging studies (24, 25). In the third measurement, for each cell the hydrogen flow was terminated (Ar only) while the cell remained polarized. The materials on the anode were electrochemically oxidized, and the time dependence and duration of the temperature increase reflected the type and amount of materials on the anode. Although the initial temperature increases (2–3°C) were similar for cells operated with either fuel, the temperature remained elevated for a longer time in the cell that had been operated with propane. This observation reflected the fact that carbon, in addition to nickel, was being oxidized. Only nickel was available for oxidation in cells operated with hydrogen. Data also showed a small but reproducible second temperature maximum at ~5 min, which probably corresponded to a peak in carbon oxidation (28). On the basis of the studies cited above, both MIR and NIR thermal imaging studies have proven to be very sensitive to temperature changes across SOFC surfaces, and these techniques also appear to have a large dynamic range. As other conditions—including those that promote more complicated chemistry—are studied, thermal imaging will continue to offer a unique view into how the resulting fuel cell processes affect SOFC operation.

4. IN SITU VIBRATIONAL SPECTROSCOPY

4.1. Motivation

Thermal imaging holds great promise for identifying spatial variations in the thermal processes that occur across SOFC electrodes, but it cannot identify the species present during SOFC operation. For example, thermal imaging cannot ascertain whether observed variations in temperature are due to graphite formation, current flow, material phase changes, or the buildup of individual intermediates formed during fuel oxidation or O_2 reduction. Spectroscopic methods—especially those that use vibrational spectroscopy—are uniquely well suited for in situ observation of specific molecular and material species. Vibrational spectroscopy has recently been used to identify in situ and real-time changes in the molecular and material composition of SOFC anodes and cathodes (26, 27, 69, 109–111, 129–131), and these studies have begun both to establish relationships between cell operating conditions and phase transformations and to explain how carbon formation affects overall cell performance.

4.2. Optical Spectroscopy: Methods and Considerations

Unlike scattering and ionization techniques that identify the stoichiometry, structure, and oxidation state(s) of elements in materials, various types of optical spectroscopies can be used to detect and unambiguously identify material structure and molecular species as well as the distributions of active and inactive sites across an electrocatalytic sample. Furthermore, optical spectroscopy is capable of standoff detection and thus can noninvasively study the processes that occur in SOFCs in situ and in real time. Of the two most common types of optical spectroscopy, electronic and vibrational, the latter has thus far shown the greatest promise for identifying chemical changes occurring in SOFCs under standard operating conditions. The appeal of vibrational spectroscopy (both IR emission and Raman scattering) is their ability to detect and clearly identify functional group compositions as well as specific phonon modes that reveal the composition and phases of solid materials.

IR and Raman spectroscopies measure the energies associated with vibrational transitions in molecules or phonon transitions in materials. IR-active transitions occur when molecules absorb or emit photons whose energy matches the energy separation between states of vibrational or lattice modes. Depending on the species being examined, IR transitions can be quite strong, and IR absorption spectra can be acquired on a routine basis from various types of samples including surfaces, thin films, and powders. Drawbacks to IR spectroscopy include a scarcity of suitable optical materials that can transmit at wavelengths longer than 3 μm. Additionally, IR detectors are not as sensitive as detectors used to measure signals in the visible region, and the dynamic range of IR detectors can be saturated by black-body radiation emanating from high-temperature sources. The latter consideration is especially pertinent to SOFC applications.

The Raman effect describes a scattering process whereby (*a*) focused, narrow-band, incident light transfers vibrational population in a molecule or material and (*b*) the energy of the resulting scattered light is equal to that of the incident light plus energy transferred into or out of the sample. Advantages of Raman spectroscopy include the ability to use conventional optics and detectors matched to the ultraviolet, visible, and/or NIR regions of the spectrum and the sensitivity of the Raman spectroscopy to low-frequency vibrations ($\geq$100 cm^{-1}). An additional advantage of using visible excitation light is that Raman spectrometers can be readily integrated into microscope assemblies via conventional imaging optics. This capability enables Raman imaging spectrometers to acquire spectra from different, well-defined, identifiable regions of heterogeneous samples with spatial resolutions of $\sim\lambda/2$ or $\sim$200 nm (132). The resolution of Raman imaging is attractive because images can contain material-specific information (in the form of vibrational transitions and relative intensities) with a spatial resolution that is relevant to the proposed length scales of electrocatalytic activity (40, 41). A schematic of an SOFC device designed for in situ Raman microscopy experiments is shown in **Figure 4**.

4.3. Infrared and Raman Studies of Solid-Oxide Fuel Cell Materials and Electrochemistry

Given the high operating temperatures of SOFCs, passive IR emission is a convenient way to learn about species present during operation. In fact, the first application of optical spectroscopy (26) to study SOFC chemistry in situ monitored the MIR emission from a samarium-doped strontium cobaltate cathode ($Sm_{0.5}Sr_{0.5}CoO_{3-\delta}$) of a SOFC button cell operating at 550°C. Liu and coworkers (26) directed the emission from a symmetric SOFC design directly into a commercial FTIR spectrometer. Vibrational-band intensities observed near 1100 cm^{-1} were assigned to the formation of superoxide (O_2^-) adsorbates (**Figure 5**). Vibrational spectra were monitored as a function of gas composition (air, 1% O_2 in N_2, and pure N_2) and as a function of cell polarization. From these data, the authors inferred that O_2^- is adsorbed at or near positively charged sites at OCV and that as cell overpotential increases, the O_2^- gradually converts to O^{2-}. These studies were groundbreaking because they established the viability of using species-specific optical methods to provide insight into the molecular processes that occur on SOFC surfaces. Furthermore, the data established clear correlations between species observed in situ with electrochemical performance.

In recent years, Raman spectroscopy has become a popular means of studying the properties of materials commonly used in SOFCs under conditions intended to reproduce those found in functioning devices (27, 109, 110, 130). Although such studies cannot directly address questions pertaining to O_2 reduction or fuel oxidation mechanisms, they can identify diagnostics that can be used to characterize processes that occur in operating SOFCs. One of the first studies that used Raman spectroscopy to study SOFC materials was reported by Pomfret et al. (27) in 2006. In this

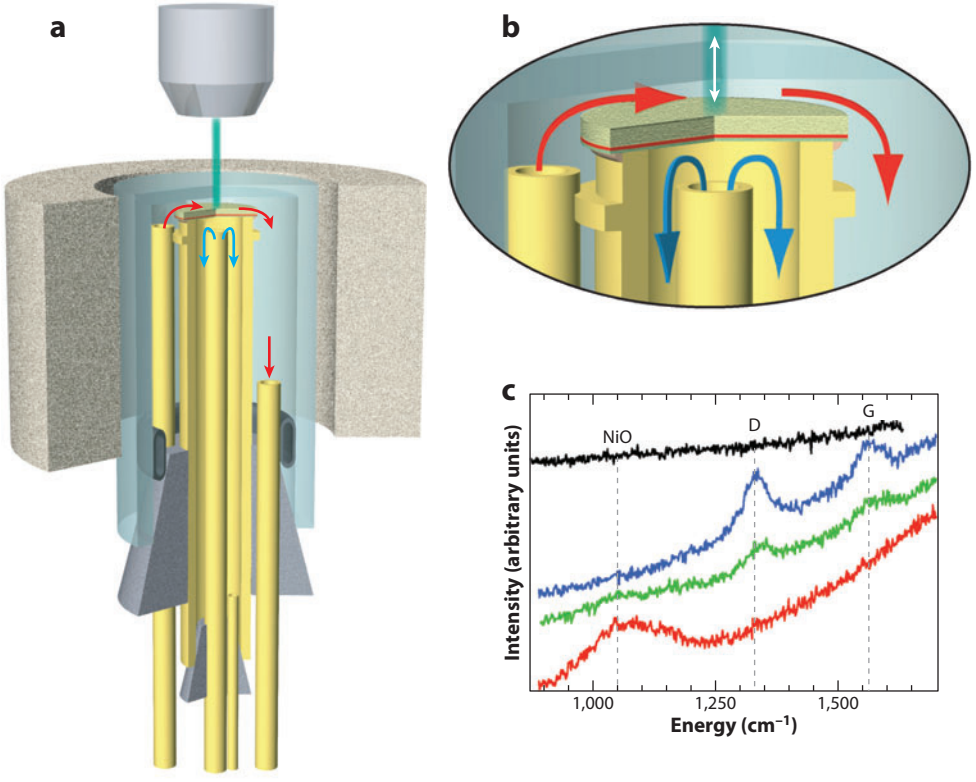

Figure 4

Schematic diagram of (*a*) the apparatus for in situ Raman microscopy of solid-oxide fuel cells, showing (*b*) a close-up of the cell and (*c*) Raman spectra of a Ni/YSZ (yttria-stabilized zirconia) cermet at 715°C. The spectra show the evolution of the surface composition due to the introduction of different gases. The top trace on panel *c* is the featureless Raman spectrum of a Ni/YSZ cermet anode. Graphite was formed from exposure to butane, as indicated by the appearance of the D and G bands (*blue spectrum*). The green spectrum shows partial removal of the carbon and Ni oxidation after 3 min of exposure to a humidified (4% H_2O) Ar flow. Further exposure to this gas mixture removes all graphite and fully oxidizes the Ni cermet anode. Spectra adapted with permission from Reference 27. Copyright 2006, American Chemical Society. Solid-oxide fuel cell drawings provided courtesy of Prof. Robert Kee.

experiment, the investigators used Raman excitation at 488 nm to monitor changes in SOFC-relevant materials at 715°C. These studies led to a Raman thermometry scale associated with temperature-dependent shifts in the F_{2g} mode of YSZ, the kinetic examination of NiO reduction and Ni oxidation, and the oxidation by steam of graphite formed on a Ni/YSZ cermet anode (**Figure 4*b***). Subsequent experiments used in situ Raman spectroscopy to monitor the redox state of the YSZ electrolyte based on changes in the intensity of the YSZ Raman–band intensities (133). Earlier ex situ studies of YSZ had identified a surface-reduced layer on YSZ electrolytes that had been exposed to reducing atmospheres at high temperatures and then returned to room temperature (134). In situ Raman experiments demonstrated that formation of this reduced phase was reversible and that conversion between a fully oxidized surface and a surface-reduced state required no more than ~3 min at a temperature of 715°C.

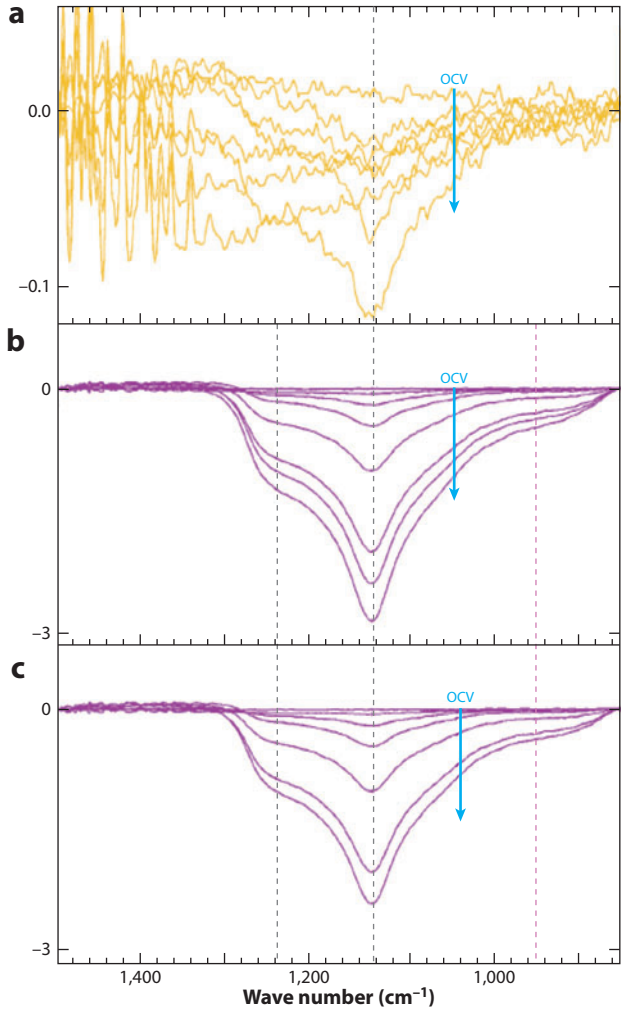

Figure 5

Fourier transform infrared spectroscopy (FTIR) emission spectra from the solid-oxide fuel cell cathode material $Sm_{0.5}Sr_{0.5}CoO_{3-\delta}$. The data have been baseline corrected, eliminating the broad black-body emission so that the narrower molecular bands are easier to observe. The spectra are measured with various gas feeds and for a range of increasing overpotentials (which increase in the direction of the arrow in each panel): (*a*) air, 0 to 320 mV; (*b*) 1% O_2 in N_2, 0 to 760 mV; and (*c*) N_2, 0 to 690 mV. The bands at 1124 cm^{-1} and 1126 cm^{-1} are assigned to various forms of superoxide, and the band at 930 cm^{-1} is attributed to peroxide anions. Abbreviation: OCV, open-circuit voltage. Figure reproduced with permission from Reference 26. Copyright 2002, the Electrochemical Society.

Like the IR experiments of Liu and coworkers (26), these Raman studies demonstrated the viability of using optical spectroscopy to study materials and processes relevant to SOFC chemistry and at standard SOFC operating temperatures. More recent results from Liu and coworkers (110) and Maher et al. (130) reported phase changes in SOFC electrode materials at temperatures approaching 600°C. Liu and colleagues (110) measured the reversible formation of different

nickel-sulfide phases from porous Ni cermet anodes exposed to small amounts of sulfur (in Ar). These results agreed well with predictions from ab initio calculations of small nickel-sulfide structures and allowed researchers to assign specific phases of the new materials formed (135). Similarly, Maher et al. (130) observed phase changes at 600°C in GDC depending on whether the atmosphere was reducing or oxidizing. These studies also clearly showed that specific material phonon-vibrational transitions change with temperature. Correlating these changes in frequency with temperature allowed researchers to determine surface temperatures with accuracies of $\leq$1°C simply by measuring a Raman spectrum. Representative figures from References 110, 130, and 133 appear in **Figure 6**.

The first application of Raman spectroscopy for the study of high-temperature chemistry on surfaces under potential control was reported in 2005 by Sum et al. (131). In these experiments, oxygen reduction in SOFC half-cell devices was monitored, albeit at temperatures significantly lower (300–500°C) than those of operational SOFCs. Raman spectra clearly showed that the center frequency and line width of the PtO vibrational band correlated with the operating voltage of the device. These experiments provided additional details about cathode chemistry that may occur in SOFCs, where Pt is often used as the electrocatalyst that reduces O_2 to O^{2-}.

The first reports of in situ optical studies of chemistry occurring in operating SOFCs—not simply in half-cells or in samples containing SOFC-relevant materials—appeared in 2007, when Pomfret et al. (111) measured the formation of graphite produced by a butane fuel feed passing over a Ni/YSZ cermet anode in a polarized SOFC. Raman spectra showed that small amounts of butane produced a mixture of ordered and disordered graphite when the SOFC was held at OCV. When the cell was operating at well-defined overpotentials, the distribution of ordered and disordered graphite changed: The ordered graphite appeared more persistent, and the disordered graphite was more labile (**Figure 7**). Graphite formation was correlated with overall SOFC performance, as demonstrated by voltammetry and impedance data.

These results addressed several issues regarding SOFC operation with carbon-containing fuels. In 2003, McIntosh et al. (9) reported that SOFCs with Cu/ceria anodes showed enhanced performance with H_2 as a benchmark fuel after having been operated with butane for several hours. The authors proposed that conducting, carbonaceous deposits formed by the incident fuel improved the connectivity of isolated metal islands in the porous anode, which increased the effective anode collection area (22). However, the in situ nature of these deposits remained uncertain. Further complicating the picture was the fact that butane pyrolyzes under typical SOFC conditions to form a mixture that includes CH_4 (36%), C_2H_4 (40%), and C_3H_6 (13%) (69, 136). Additional experiments by Pomfret et al. (137) examined the effects of individual hydrocarbon fuels on SOFC performance and found that the curious electrochemical behavior first reported by McIntosh et al. (9) required that both ethylene and propylene be present in the fuel mixture. Neither fuel by itself led to the same type and rate of graphite formation nor to the same electrochemical performance.

Given the ability of optical spectroscopy to measure solid-state structure, the presence of molecular intermediates, and the kinetics of electrochemical processes in situ, these methods will probably be increasingly applied to the study of chemistry that occurs in SOFCs. Both existing and new experimental programs will be able to characterize the oxidation and degradation mechanisms that control electrochemical performance of diverse fuels on a wide variety of electrocatalytic materials. The resulting data will be useful for testing electrochemical oxidation models and anode-degradation mechanisms for a variety of fuels (including oxygenated, synthetic, and bioderived fuels) and contaminants (including sulfur, silica, and iron).

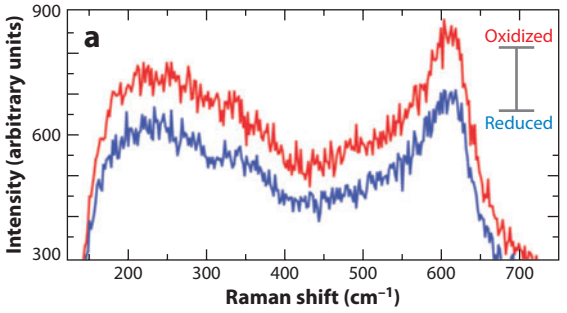

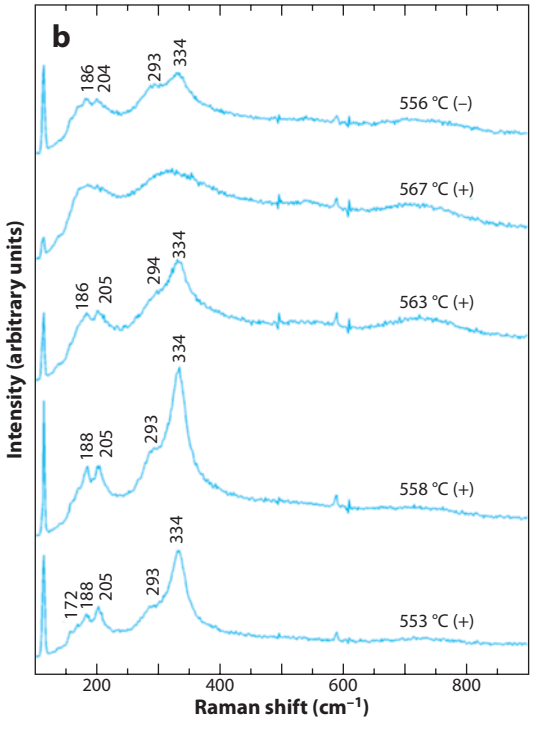

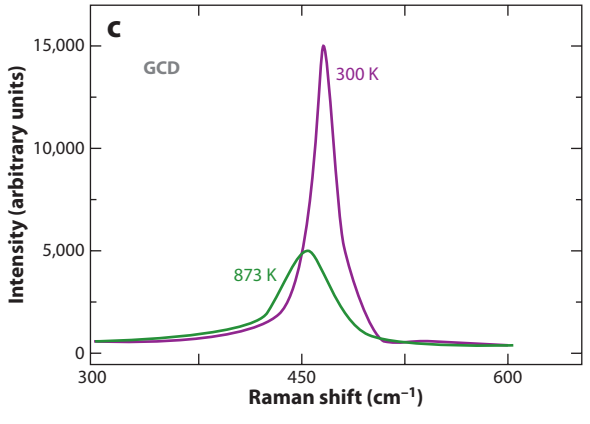

5. SUMMARY AND OUTLOOK

Given the need for efficient sources of electrical power that can use a wide variety of fuels, SOFCs are poised to become an increasingly important part of the world's energy-production infrastructure. This anticipated growth provides clear motivation for the development and application of techniques that can identify, in situ and in real time, the chemistry that occurs in SOFCs. Therefore, in situ optical diagnostics that provide molecular and spatial specificity will enable scientists and engineers to more readily evaluate models and understand electrochemical operation in high-temperature environments. A synergistic relationship among in situ optical studies, kinetic modeling, and advances in SOFC materials and architectures will improve device durability and efficiency.

In the larger context of SOFC research, experimental measurements that can identify chemical species as a function of operating conditions have been limited. This review examines a growing collection of optical methods that have begun to provide information and insight into (*a*) the mechanisms responsible for oxide formation at cathodes, (*b*) the dependence of carbon deposition on fuel identity, and (*c*) the impact of carbon deposition and other contaminants on overall SOFC performance. IR emission and in situ Raman spectroscopy promise to deepen our understanding of both cathode and anode chemistry under a wide range of conditions. The growing number of studies from researchers around the world has begun to provide the quantitative, direct information necessary to spur the development and refinement of predictive models and operational protocols. Further improvement of these techniques for in situ studies will result from the use of shorter-wavelength excitation sources for Raman spectroscopy and the use of IR emission and reflection from anodes, where the expected molecular species, such as CO and CO_2, should have large IR transition moments. Furthermore, techniques established for in situ proton-exchange membrane studies (138) and for high-temperature solid-state materials (139), as well as for different types of electronic spectroscopy (e.g., fluorescence), are expected to provide additional insight into SOFC chemistry occurring in situ.

Additional advances will probably result from combining imaging and spectroscopy. For example, various types of hyperspectral imaging that are well established in remote sensing and are now being employed in other areas, such as combustion and bioimaging, are particularly attractive for SOFC studies because they combine the benefits of imaging and spectroscopy to simultaneously achieve both spatial and molecular resolution (140–143). Hopefully, lessons learned from studies of model cells will be transferable so that in situ optical techniques can be integrated into process-monitoring systems that provide feedback and damage control for commercial systems.

Figure 6

Raman spectra of various materials relevant to solid-oxide fuel cells. (*a*) The reversible changes in intensity of an yttria-stabilized zirconia electrolyte depending on whether the sample is exposed to air (*red*) or to 5% H_2 in Ar (*blue*). Spectra were acquired at a temperature of 715°C with 488-nm excitation. Adapted with permission from Reference 133. Copyright 2008, The Electrochemical Society. (*b*) The onset of the cubic phase of Ni_3S_2 (at 567°C), as evidenced by the loss of intensity in the feature at 334 cm^{-1} assigned to the Ni_3S_2 rhombohedral phase. Cooling the sample back to 556°C (*top spectrum*) allowed the return of the 334 cm^{-1} band, demonstrating that the transition is reversible. Spectra were collected with 514-nm excitation. Data reproduced with permission from Reference 110. Copyright 2007, American Chemical Society. (*c*) Raman spectra obtained from gadolinium-doped ceria (GDC) at room temperature and at 600°C by means of a 633-nm excitation source. Reproduced with permission from Reference 130. Copyright 2008, American Chemical Society.

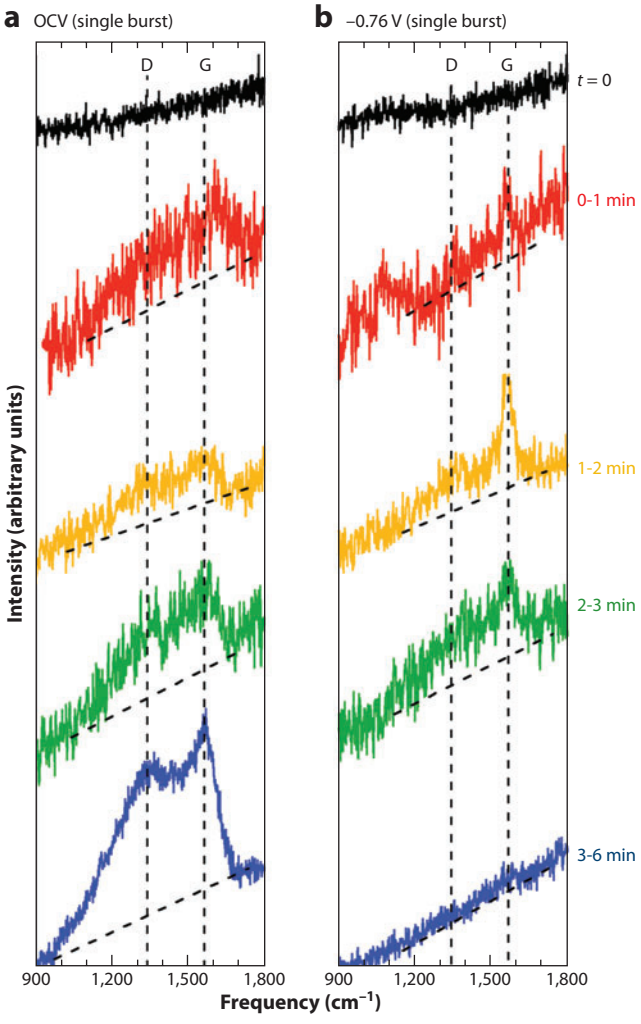

Figure 7

Raman spectra acquired from a Ni/YSZ (yttria-stabilized zirconia) anode of a YSZ-supported button cell operating at (*a*) −1.06 V [open-circuit voltage (OCV)] and (*b*) −0.76 V. Each experiment was carried out at 715°C and used 488-nm excitation. In each experiment, the anode was exposed to a continuous flow of H_2 in Ar. To this feed, 5 cc of butane was added at time $t = 0$. Spectra were then acquired every minute. The appearance of the D and G bands indicates the formation of graphite. When the cell was drawing a current (−0.76 V), the graphite disappeared over time. At OCV, the graphite persisted indefinitely. Data adapted with permission from Reference 111. Copyright 2007, American Chemical Society.

DISCLOSURE STATEMENT

The authors are not aware of any affiliations, memberships, funding, or financial holdings that might be perceived as affecting the objectivity of this review.

ACKNOWLEDGMENTS

The authors' work is supported by the Office of Naval Research. The authors specifically thank Professors Bryan W. Eichhorn and Gregory S. Jackson at the University of Maryland for insightful

discussions and Professor Robert J. Kee at the Colorado School of Mines for graciously providing the illustrations in **Figures 2** and **4**. The authors also thank Professor Meilin Liu at the Georgia Institute of Technology and Dr. Robert Maher and Professor Nigel Brandon at Imperial College London for permission to reproduce data from References 24, 26, 110, and 130.

LITERATURE CITED

1. Grove WR. 1838. On a new voltaic combination. *Philos. Mag. J. Sci.* 13:430
2. Ormerod RM. 2003. Solid oxide fuel cells. *Chem. Soc. Rev.* 32:17–28
3. Brett DJL, Atkinson A, Brandon NP, Skinner SJ. 2008. Intermediate temperature solid oxide fuel cells. *Chem. Soc. Rev.* 37:1568–78
4. Atkinson A, Barnett S, Gorte RJ, Irvine JTS, McEvoy AJ, et al. 2004. Advanced anodes for high-temperature fuel cells. *Nat. Mater.* 3:17–27
5. Minh NQ. 2004. Solid oxide fuel cell technology-features and applications. *Solid State Ion.* 174:271–77
6. Kendall K. 2005. Progress in solid oxide fuel cell materials. *Int. Mater. Rev.* 50:257–64
7. EG&G Technical Services Inc. 2004. *Fuel Cell Handbook*. Morgantown: US Dep. Energy. 7th ed. **http://www.cleanfuelcellenergy.com/FCHandbook7.pdf**
8. Goodenough JB. 2003. Oxide-ion electrolytes. *Annu. Rev. Mater. Res.* 33:91–128
9. McIntosh S, Vohs JM, Gorte RJ. 2003. Role of hydrocarbon deposits in the enhanced performance of direct-oxidation SOFCs. *J. Electrochem. Soc.* 150:A470–76
10. Mogensen M, Kammer K. 2003. Conversion of hydrocarbons in solid oxide fuel cells. *Annu. Rev. Mater. Res.* 33:321–31
11. Verma A, Rao AD, Samuelsen GS. 2006. Sensitivity analysis of a Vision 21 coal based zero emission power plant. *J. Power Sources* 158:417–27
12. Gorte RJ, Park S, Vohs JM, Wang CH. 2000. Anodes for direct oxidation of dry hydrocarbons in a solid-oxide fuel cell. *Adv. Mater.* 12:1465–69
13. Aguadero A, de la Calle C, Alonso JA, Perez-Coll D, Escudero MJ, Daza L. 2009. Structure, thermal stability and electrical properties of $Ca(V_{0.5}Mo_{0.5})O_3$ as solid oxide fuel cell anode. *J. Power Sources* 192:78–83
14. Bebelis S, Neophytides S. 2002. AC impedance study of Ni-YSZ cermet anodes in methane-fuelled internal reforming YSZ fuel cells. *Solid State Ion.* 152–53:447–53
15. Castro EB, Giz MJ, Gonzalez ER, Vilche JR. 1997. An electrochemical impedance study on the kinetics and mechanism of the hydrogen evolution reaction on nickel molybdenite electrodes. *Electrochim. Acta* 42:951–59
16. Diethelm S, Closset A, Van Herle J, Nisancioglu K. 2002. Determination of chemical diffusion and surface exchange coefficients of oxygen by electrochemical impedance spectroscopy. *J. Electroanal. Chem.* 149:E424–32
17. Lauvstad GO, Tunold R, Sunde S. 2002. Electrochemical oxidation of CO on Pt and Ni point electrodes in contact with an yttria-stabilized zirconia electrolyte. II. Steady-state and impedance measurements. *J. Electrochem. Soc.* 149:E506–14
18. Narita H, Mizusaki J, Tagawa H. 1993. Characteristic impedance spectrum associated with partial reduction of electrolyte and/or electrode of zirconia cells. *Denki Kagaku* 61:756
19. Norinaga K, Deutschmann O. 2007. Detailed kinetic modeling of gas-phase reactions in the chemical vapor deposition of carbon from light hydrocarbons. *Ind. Eng. Chem. Res.* 46:3547–57
20. Randolph KL, Dean AM. 2007. Hydrocarbon fuel effects in solid-oxide fuel cell operation: an experimental and modeling study of n-hexane pyrolysis. *Phys. Chem. Chem. Phys.* 9:4245–58
21. Yi J, Kaloyannis A, Vayenas CG. 1993. High-temperature cyclic voltammetry of Pt catalyst-electrodes in solid-electrolyte cells. *Electrochim. Acta* 38:2533–39
22. McIntosh S, He HP, Lee SI, Costa-Nunes O, Krishnan VV, et al. 2004. An examination of carbonaceous deposits in direct-utilization SOFC anodes. *J. Electrochem. Soc.* 151:A604–8
23. Tikekar NM, Armstrong TJ, Virkar AV. 2006. Reduction and reoxidation kinetics of nickel-based SOFC anodes. *J. Electrochem. Soc.* 153:A654–63

24. Brett DJL, Aguiar P, Clague R, Marquis AJ, Schottl S, et al. 2007. Application of infrared thermal imaging to the study of pellet solid oxide fuel cells. *J. Power Sources* 166:112–19
25. Ju G, Reifsnider K, Xinyu H. 2008. Infrared thermography and thermoelectrical study of a solid oxide fuel cell. *J. Fuel Cell Sci. Technol.* 5:031006
26. Lu XY, Faguy PW, Liu ML. 2002. In situ potential-dependent FTIR emission spectroscopy—a novel probe for high temperature fuel cell interfaces. *J. Electrochem. Soc.* 149:A1293–98
27. Pomfret MB, Owrutsky JC, Walker RA. 2006. High-temperature Raman spectroscopy of solid oxide fuel cell materials and processes. *J. Phys. Chem. B* 110:17305–8
28. Pomfret MB, Steinhurst DA, Kidwell DA, Owrutsky JC. 2010. Thermal imaging of SOFC anode processes. *J. Power Sources* 195:257–62
29. Bi ZH, Zhu JH. 2009. A Cu-CeO_2-LDC composite anode for LSGM electrolyte-supported solid oxide fuel cells. *Electrochem. Solid State Lett.* 12:B107–11
30. Fergus JW. 2006. Electrolytes for solid oxide fuel cells. *J. Power Sources* 162:30–40
31. Gong W, Gopalan S, Pal UB. 2005. Materials system for intermediate-temperature (600–800°C) SOFCs based on doped lanthanum-gallate electrolyte. *J. Electrochem. Soc.* 152:A1890–95
32. Rupp JLM, Drobek T, Rossi A, Gauckler LJ. 2007. Chemical analysis of spray pyrolysis gadolinia-doped ceria electrolyte thin films for solid oxide fuel cells. *Chem. Mater.* 19:1134–42
33. Song HZ, Wang HB, Zha SW, Peng DK, Meng GY. 2003. Aerosol-assisted MOCVD growth of Gd_2O_3-doped CeO_2 thin SOFC electrolyte film on anode substrate. *Solid State Ion.* 156:249–54
34. Wang C, Xui LH, Tang WH. 2006. Study on SGDC electrolyte film prepared by RF magnetron sputtering. *Rare Metal Mater. Eng.* 35:501–3
35. Zhang X, Robertson M, Deces-Petit C, Qu W, Kesler O, et al. 2007. Internal shorting and fuel loss of a low temperature solid oxide fuel cell with SDC electrolyte. *J. Power Sources* 164:668–77
36. Jiang SP. 2008. Development of lanthanum strontium manganite perovskite cathode materials of solid oxide fuel cells: a review. *J. Mater. Sci.* 43:6799–833
37. Julien C, Letranchant C, Rangan S, Lemal M, Ziolkiewicz S, et al. 2000. Layered $LiNi_{0.5}Co_{0.5}O_2$ cathode materials grown by soft-chemistry via various solution methods. *Mater. Sci. Engin. B.* 76:145–55
38. Li Q, Zhao H, Huo LH, Sun LP, Cheng XL, Grenier JC. 2007. Electrode properties of Sr doped La_2CuO_4 as new cathode material for intermediate-temperature SOFCs. *Electrochem. Commun.* 9:1508–12
39. Liu Y. 2009. $YBaCo_2O_{5+\delta}$ as a new cathode material for zirconia-based solid oxide fuel cells. *J. Alloys Compd.* 477:860–62
40. Mai A, Haanappel VAC, Uhlenbruck S, Tietz F, Stover D. 2005. Ferrite-based perovskites as cathode materials for anode-supported solid oxide fuel cells. Part I. Variation of composition. *Solid State Ion.* 176:1341–50
41. Ralph JM, Rossignol C, Kumar R. 2003. Cathode materials for reduced-temperature SOFCs. *J. Electrochem. Soc.* 150:A1518–22
42. Wang C-L, Sun X-L, Li S, Ji S-J, Sun J-C. 2008. New cathode material $LaNi_{0.8}Cu_{0.2}O_3$ for low temperature solid oxide fuel cell. *Chin. J. Power Sources*:177–79
43. Zhao HL, Teng DQ, Zhang XH, Zhang CJ, Li X. 2009. Structural and electrochemical studies of $Ba_{0.6}Sr_{0.4}Co_{1-y}Ti_yO_{3-\delta}$ as a new cathode material for IT-SOFCs. *J. Power Sources* 186:305–10
44. Zheng Y, Zhang C, Ran R, Cai R, Shao ZP, Farrusseng D. 2009. A new symmetric solid-oxide fuel cell with $La_{0.8}Sr_{0.2}Sc_{0.2}Mn_{0.8}O_{3-\delta}$ perovskite oxide as both the anode and cathode. *Acta Mater.* 57:1165–75
45. Adcock PA, Pacheco SV, Norman KM, Uribe FA. 2005. Transition metal oxides as reconfigured fuel cell anode catalysts for improved CO tolerance: polarization data. *J. Electrochem. Soc.* 152:A459–66
46. Bao WT, Guan HM, Cheng JH. 2008. A new anode material for intermediate solid oxide fuel cells. *J. Power Sources* 175:232–37
47. Gong MY, Liu XB, Trembly J, Johnson C. 2007. Sulfur-tolerant anode materials for solid oxide fuel cell application. *J. Power Sources* 168:289–98
48. Goodenough JB, Huang YH. 2007. Alternative anode materials for solid oxide fuel cells. *J. Power Sources* 173:1–10
49. Huang YH, Liang G, Croft M, Lehtimäki M, Karppinen M, Goodenough JB. 2009. Double-perovskite anode materials Sr_2MMoO_6 (M = Co, Ni) for solid oxide fuel cells. *Chem. Mater.* 21:2319–26

50. Ishihara T, Yan JW, Shinagawa M, Matsumoto H. 2006. Ni-Fe bimetallic anode as an active anode for intermediate temperature SOFC using $LaGaO_3$ based electrolyte film. *Electrochim. Acta* 52:1645–50
51. Jiang SP, Chan SH. 2004. A review of anode materials development in solid oxide fuel cells. *J. Mater. Sci.* 39:4405–39
52. Kurokawa H, Sholklapper TZ, Jacobson CP, De Jonghe LC, Visco SJ. 2007. Ceria nanocoating for sulfur tolerant Ni-based anodes of solid oxide fuel cells. *Electrochem. Solid State Lett.* 10:B135–38
53. Liu J, Madsen BD, Ji Z, Barnett SA. 2002. A fuel-flexible ceramic-based anode for solid oxide fuel cells. *Electrochem. Solid-State Lett.* 5:A122–24
54. Lu XC, Zhu JH. 2008. Amorphous ceramic material as sulfur-tolerant anode for SOFC. *J. Electrochem. Soc.* 155:B1053–57
55. Lv H, Yang DJ, Pan XM, Zheng JS, Zhang CM, et al. 2009. Performance of Ce/Fe oxide anodes for SOFC operating on methane fuel. *Mater. Res. Bull.* 44:1244–48
56. Putna ES, Stubenrauch J, Vohs JM, Gorte RJ. 1995. Ceria-based anodes for the direct oxidation of methane in solid oxide fuel cells. *Langmuir* 11:4832–37
57. Sin A, Kopnin E, Dubitsky Y, Zaopo A, Arico AS, et al. 2007. Performance and life-time behaviour of NiCu-CGO anodes for the direct electro-oxidation of methane in IT-SOFCs. *J. Power Sources* 164:300–5
58. Wang FY, Jung GB, Su A, Chan SH, Hao X, Chiang YC. 2008. Porous Ag-$Ce_{0.8}Sm_{0.2}O_{1.9}$ cermets as anode materials for intermediate temperature solid oxide fuel cells using CO fuel. *J. Power Sources* 185:862–66
59. Xu ZR, Luo JL, Chuang KT, Sanger AR. 2007. $LaCrO_3$-VO_x-YSZ anode catalyst for solid oxide fuel cell using impure hydrogen. *J. Phys. Chem. C* 111:16679–85
60. Ye XF, Huang B, Wang SR, Wang ZR, Xiong L, Wen TL. 2007. Preparation and performance of a Cu-CeO_2-ScSZ composite anode for SOFCs running on ethanol fuel. *J. Power Sources* 164:203–9
61. Hirabayashi D, Hashimoto A, Hibino T, Harada U, Sano M. 2004. Bi-based oxide anodes for direct hydrocarbon SOFCs at intermediate temperatures. *Electrochem. Solid State Lett.* 7:A108–10
62. Lin YB, Zhan ZL, Liu J, Barnett SA. 2005. Direct operation of solid oxide fuel cells with methane fuel. *Solid State Ion.* 176:1827–35
63. Nabae Y, Yamanaka I, Hatano M, Otsuka K. 2006. Catalytic behavior of Pd-Ni/composite anode for direct oxidation of methane in SOFCs. *J. Electrochem. Soc.* 153:A140–45
64. Walters KM, Dean AM, Zhu HY, Kee RJ. 2003. Homogeneous kinetics and equilibrium predictions of coking propensity in the anode channels of direct oxidation solid-oxide fuel cells using dry natural gas. *J. Power Sources* 123:182–89
65. Gorte RJ, Kim H, Vohs JM. 2002. Novel SOFC anodes for the direct electrochemical oxidation of hydrocarbon. *J. Power Sources* 106:10–15
66. Kee RJ, Zhu HY, Goodwin DG. 2005. Solid-oxide fuel cells with hydrocarbon fuels. *Proc. Combust. Inst.* 30:2379–404
67. Kim T, Liu G, Boaro M, Lee SI, Vohs JM, et al. 2006. A study of carbon formation and prevention in hydrocarbon-fueled SOFC. *J. Power Sources* 155:231–38
68. Liu J. 2006. Direct-hydrocarbon solid oxide fuel cells. *Prog. Chem.* 18:1026–33
69. Pomfret MB, Marda J, Jackson GS, Eichhorn BW, Dean AM, Walker RA. 2008. Hydrocarbon fuels in solid oxide fuel cells: in situ Raman studies of graphite formation and oxidation. *J. Phys. Chem. C* 112:5232–40
70. Cimenti M, Hill JM. 2009. Thermodynamic analysis of solid oxide fuel cells operated with methanol and ethanol under direct utilization, steam reforming, dry reforming or partial oxidation conditions. *J. Power Sources* 186:377–84
71. Faungnawakij K, Kikuchi R, Eguchi K. 2007. Thermodynamic analysis of carbon formation boundary and reforming performance for steam reforming of dimethyl ether. *J. Power Sources* 164:73–79
72. Laosiripojana N, Assabumrungrat S. 2007. Catalytic steam reforming of methane, methanol, and ethanol over Ni/YSZ: The possible use of these fuels in internal reforming SOFC. *J. Power Sources* 163:943–51
73. Mathieu DM, Dean AM, Grenda JM, Green JWH. 2003. Mechanism generation with integrated pressure dependance: a new model for methane pyrolysis. *J. Phys. Chem. A* 107:8552–68
74. Sheng CY, Dean AM. 2004. Importance of gas-phase kinetics within the anode channel of a solid-oxide fuel cell. *J. Phys. Chem. A* 108:3772–83

75. Sheng CY, Dean AM. 2003. *Comparison of experimental results to model predictions for n-butane pyrolysis under high-temperature fuel cell conditions*. Presented at Jt. Meet. U.S. Sect. Combust. Inst., 3rd, Chicago
76. Braun A, Janousch M, Sfeir J, Kiviaho J, Noponen M, et al. 2008. Molecular speciation of sulfur in solid oxide fuel cell anodes with X-ray absorption spectroscopy. *J. Power Sources* 183:564–70
77. Cheng Z, Liu ML. 2007. Characterization of sulfur poisoning of Ni-YSZ anodes for solid oxide fuel cells using in situ Raman micro spectroscopy. *Solid State Ion.* 178:925–35
78. Offer GJ, Mermelstein J, Brightman E, Brandon NP. 2009. Thermodynamics and kinetics of the interaction of carbon and sulfur with solid oxide fuel cell anodes. *J. Am. Ceram. Soc.* 92:763–80
79. Bieberle A, Gauckler LJ. 2002. State-space modeling of the anodic SOFC system Ni, H_2-H_2O vertical bar YSZ. *Solid State Ion.* 146:23–41
80. Bove R, Lunghi P, Sammes NM. 2005. SOFC mathernatic model for systems simulations. Part One: from a micro-detailed to macro-black-box model. *Int. J. Hydrog. Energy* 30:181–87
81. Bove R, Ubertini S. 2006. Modeling solid oxide fuel cell operation: approaches, techniques and results. *J. Power Sources* 159:543–59
82. Chaisantikulwat A, Diaz-Goano C, Meadows ES. 2008. Dynamic modelling and control of planar anode-supported solid oxide fuel cell. *Comp. Chem. Eng.* 32:2365–81
83. Choi Y, Mebane DS, Wang JH, Liu M. 2007. Continuum and quantum-chemical modeling of oxygen reduction on the cathode in a solid oxide fuel cell. *Top. Catal.* 46:386–401
84. DeCaluwe SC, Zhu H, Kee RJ, Jackson GS. 2008. Importance of anode microstructure in modeling solid oxide fuel cells. *J. Electrochem. Soc.* 155:B538–46
85. Fleig J. 2003. Solid oxide fuel cell cathodes: polarization mechanisms and modeling of the electrochemical performance. *Annu. Rev. Mater. Res.* 33:361–82
86. Huang QA, Hui R, Wang BW, Zhang HJ. 2007. A review of AC impedance modeling and validation in SOFC diagnosis. *Electrochim. Acta* 52:8144–64
87. Kakac S, Pramuanjaroenkij A, Zhou XY. 2007. A review of numerical modeling of solid oxide fuel cells. *Int. J. Hydrog. Energy* 32:761–86
88. Ma L, Ingham DB, Pourkashanian M, Carcadea E. 2005. Review of the computational fluid dynamics modeling of fuel cells. *J. Fuel Cell Sci. Technol.* 2:246–57
89. Mitterdorfer A, Gauckler LJ. 1999. Identification of the reaction mechanism of the Pt, $O_{2(g)}$ vertical bar yttria-stabilized zirconia system. Part II: Model implementation, parameter estimation, and validation. *Solid State Ion.* 117:203–17
90. Morel B, Laurencin J, Bultel Y, Lefebvre-Joud F. 2005. Anode-supported SOFC model centered on the direct internal reforming. *J. Electrochem. Soc.* 152:A1382–89
91. Nam JH, Jeon DH. 2006. A comprehensive micro-scale model for transport and reaction in intermediate temperature solid oxide fuel cells. *Electrochim. Acta* 51:3446–60
92. Svensson AM, Sunde S, Nisancioglu K. 1997. Mathematical modeling of oxygen exchange and transport in air-perovskite-YSZ interface regions. I. Reduction of intermediately adsorbed oxygen. *J. Electrochem. Soc.* 144:2719–32
93. Zhu HY, Kee RJ. 2006. Modeling electrochemical impedance spectra in SOFC button cells with internal methane reforming. *J. Electrochem. Soc.* 153:A1765–72
94. Goldin GM, Zhu H, Kee RJ, Bierschenk D, Barnett SA. 2009. Multidimensional flow, thermal, and chemical behavior in solid-oxide fuel cell button cells. *J. Power Sources* 187:123–35
95. Hughes AE, Sexton BA. 1989. XPS study of an intergranular phase in yttria-zirconia. *J. Mater. Sci.* 24:1057–61
96. Nijhuis TA, Tinnemans SJ, Visser T, Weckhuysen BM. 2003. Operando spectroscopic investigation of supported metal oxide catalysts by combined time-resolved UV-VIS/Raman/on-line mass spectrometry. *Phys. Chem. Chem. Phys.* 5:4361–65
97. Richardson JT, Scates R, Twigg MV. 2003. X-ray diffraction study of nickel oxide reduction by hydrogen. *Appl. Catal. A* 246:137–50
98. Smith TR, Wood A, Birss VI. 2009. Effect of hydrogen sulfide on the direct internal reforming of methane in solid oxide fuel cells. *Appl. Catal. A* 354:1–7

99. Pijolat M, Caillol N, Siebert E. 2007. Investigation of chemisorbed oxygen, surface segregation and effect of post-treatments on $La_{0.8}Sr_{0.2}MnO_3$ powder and screen-printed layers for solid oxide fuel cell cathodes. *Appl. Surf. Sci.* 253:4641–48
100. Pomfret MB, Demircan O, Sukeshini AM, Walker RA. 2006. Fuel oxidation efficiencies and exhaust composition in solid oxide fuel cells. *Environ. Sci. Technol.* 40:5574–79
101. Mingjia Z, Xinqi C, Finklea H, Celik I, Wu NQ. 2008. Electrochemical and microstructural analysis of nickel-yttria-stabilized zirconia electrode operated in phosphorus-containing syngas. *J. Power Sources* 183:485–90
102. Biniwale RB, Kariya N, Yamashiro H, Ichikawa M. 2006. Heat transfer and thermographic analysis of catalyst surface during multiphase phenomena under spray-pulsed conditions for dehydrogenation of cyclohexane over Pt catalysts. *J. Phys. Chem. B* 110:3189–96
103. Hakenjos A, Muenter H, Wittstadt U, Hebling C. 2004. A PEM fuel cell for combined measurement of current and temperature distribution, and flow field flooding. *J. Power Sources* 131:213–16
104. Simeone M, Salemme L, Allouis C. 2008. Reactor temperature profile during autothermal methane reforming on Rh/Al_2O_3 catalyst by IR imaging. *Int. J. Hydrog. Energy* 33:4798–808
105. Wang M, Guo H, Ma C. 2006. Temperature distribution on the MEA surface of a PEMFC with serpentine channel flow bed. *J. Power Sources* 157:181–87
106. Kakihana M, Osada M. 2003. Raman spectroscopy as a characterization tool for carbon materials. In *Carbon Alloys: Novel Concepts to Develop Carbon Science and Technology*, ed. E Yasuda, M Inagaki, M Kaneko, M Endo, A Oya, Y Tanabe, pp. 285–97. Oxford: Elsevier
107. Xu C, Xu G, Wang G. 2002. Preparation and characterization of NiO nanorods by thermal decomposition of NiC_2O_4 precursor. *J. Mater. Sci.* 38:779–82
108. Zouboulis E, Renusch D, Grimsditch M. 1998. Advantages of ultraviolet Raman scattering for high temperature investigations. *Appl. Phys. Lett.* 72:1–3
109. Abernathy HW, Koep E, Compson C, Cheng Z, Liu ML. 2008. Monitoring Ag-Cr interactions in SOFC cathodes using Raman spectroscopy. *J. Phys. Chem. C* 112:13299–303
110. Cheng Z, Abernathy H, Liu ML. 2007. Raman spectroscopy of nickel sulfide Ni_3S_2. *J. Phys. Chem. C* 111:17997–8000
111. Pomfret MB, Owrutsky JC, Walker RA. 2007. In situ studies of fuel oxidation in solid oxide fuel cells. *Anal. Chem.* 79:2367–72
112. Farrow RL, Rakestraw DJ. 1992. Detection of trace molecular-species using degenerate 4-wave-mixing. *Science* 257:1894–900
113. Kaminski CF. 2005. Fluorescence imaging of reactive processes. *Z. Phys. Chem.* 219:747–74
114. Masri AR, Dibble RW, Barlow RS. 1996. The structure of turbulent nonpremixed flames revealed by Raman-Rayleigh-LIF measurements. *Prog. Energy Combust. Sci.* 22:307–62
115. Rothe EW, Andresen P. 1997. Application of tunable excimer lasers to combustion diagnostics: a review. *Appl. Opt.* 36:3971–4033
116. Schulz C, Sick V. 2005. Tracer-LIF diagnostics: quantitative measurement of fuel concentration, temperature and fuel/air ratio in practical combustion systems. *Prog. Energy Combust. Sci.* 31:75–121
117. Zhao H, Ladommatos N. 1998. Optical diagnostics for in-cylinder mixture formation measurements in IC engines. *Prog. Energy Combust. Sci.* 24:297–336
118. Owrutsky JC, Steinhurst DA, Minor CP, Rose-Pehrsson SL, Williams FW, Gottuk DT. 2006. Long wavelength video detection of fire in ship compartments. *Fire Safety J.* 41:315–20
119. Allison SW, Gillies GT. 1997. Remote thermometry with thermographic phosphors: instrumentation and applications. *Rev. Sci. Instrum.* 68:2615–50
120. Gentleman MM, Clarke DR. 2004. Concepts for luminescence sensing of thermal barrier coatings. *Surf. Coat. Technol.* 188–89:93–100
121. Zhu WZ, Deevi SC. 2003. A review on the status of anode materials for solid oxide fuel cells. *Mater. Sci. Engin.* 362:A228–39
122. Recknagle KP, Williford RE, Chick LA, Rector DR, Khaleel MA. 2003. Three-dimensional thermo-fluid electrochemical modeling of planar SOFC stacks. *J. Power Sources* 113:109–14
123. Adzic M, Heitor MV, Santos D. 1997. Design of dedicated instrumentation for temperature distribution measurements in solid oxide fuel cells. *J. Appl. Electrochem.* 27:1355–61

124. He SH, Mench MM, Tadigadapa S. 2006. Thin film temperature sensor for real-time measurement of electrolyte temperature in a polymer electrolyte fuel cell. *Sens. Actuators A* 125:170–77
125. Kim D, Lee J, Lim TH, Oh IH, Ha HY. 2006. Operational characteristics of a 50 W DMFC stack. *J. Power Sources* 155:203–12
126. Saito T, Sakai S, Iizawa I, Suda E, Umentani K, et al. 2005. A new technique of radiation thermometry using a consumer digital camcorder: observations of red glow at Aso Volcano, Japan. *Earth Planets Space* 57:5–8
127. Zauner G, Heim D, Hendorfer G, Niel K. 2003. Temperature mapping in heat treatment processes with a standard color-video camera by means of image processing. *Proc. SPIE* 5011:283–90
128. Csiszar IA, Morisette JT, Giglio L. 2006. Validation of active fire detection from moderate-resolution satellite sensors: the MODIS example in northern Eurasia. *IEEE Trans. Geosci. Remote Sens.* 44:1757–64
129. Dong J, Cheng Z, Zha SW, Liu ML. 2006. Identification of nickel sulfides on Ni-YSZ cermet exposed to H_2 fuel containing H_2S using Raman spectroscopy. *J. Power Sources* 156:461–65
130. Maher RC, Cohen LF, Lohsoontorn P, Brett DJL, Brandon NP. 2008. Raman spectroscopy as a probe of temperature and oxidation state for gadolinium-doped ceria used in solid oxide fuel cells. *J. Phys. Chem. A* 112:1497–501
131. Sum OSN, Djurado E, Pagnier T, Rosman N, Roux C, Siebert E. 2005. Raman investigation of the O_2, Pt/YSZ electrode under polarization. *Solid State Ion.* 176:2599–607
132. Jahncke C, Paesler M, Hallen H. 1995. Raman imaging with near-field scanning optical microscopy. *Appl. Phys. Lett.* 67:2483–85
133. Pomfret MB, Eigenbrodt BC, Walker RA. 2008. Interfacial resistivity of yttria stabilized zirconia in operating solid oxide fuel cells. *Electrochem. Soc. Trans.* 11:111–20
134. Pomfret MB, Stoltz C, Varughese B, Walker RA. 2005. Structural and compositional characterization of yttria-stabilized zirconia: evidence of surface-stabilized, low-valence metal species. *Anal. Chem.* 77:1791–95
135. Wang JH, Cheng Z, Bredas JL, Liu ML. 2007. Electronic and vibrational properties of nickel sulfides from first principles. *J. Chem. Phys.* 127:214705
136. Gupta GK, Dean AM, Ahn K, Gorte RJ. 2006. Comparison of conversion and deposit formation of ethanol and butane under SOFC conditions. *J. Power Sources* 158:497–503
137. Pomfret MB, Owrutsky JC, Walker RA. 2008. Toward a mechanistic understanding of solid oxide fuel cell chemistry through in-situ Raman spectroscopy. *Electrochem. Soc. Trans.* 11:99–109
138. Sun S-G, Christensen PA, Wieckowski A, eds. 2007. *In-Situ Spectroscopic Studies of Adsorption at the Electrode and Electrocatalysis*. Amsterdam: Elsevier
139. Goguet A, Meunier FC, Tibiletti D, Breen JP, Burch R. 2004. Spectrokinetic investigation of reverse water-gas-shift reaction intermediates over a Pt/CeO_2 catalyst. *J. Phys. Chem. B* 108:20240–46
140. Beechem T, Graham S, Kearney SP, Phinney LM, Serrano JR. 2007. Simultaneous mapping of temperature and stress in microdevices using micro-Raman spectroscopy. *Rev. Sci. Instrum.* 78:061301
141. Kohsehoinghaus K. 1994. Laser techniques for the quantitative detection of reactive intermediates in combustion systems. *Prog. Energy Combust. Sci.* 20:203–79
142. Najm HN, Paul PH, Mueller CJ, Wyckoff PS. 1998. On the adequacy of certain experimental observables as measurements of flame burning rate. *Combust. Flame* 113:312–32
143. Vo-Dinh T, Yan F, Wabuyele MB. 2005. Surface-enhanced Raman scattering for medical diagnostics and biological imaging. *J. Raman Spectrosc.* 36:640–47

Annual Review of
Analytical Chemistry

Volume 3, 2010

Contents

Indexes

Errata

An online log of corrections to *Annual Review of Analytical Chemistry* articles may be found at http://arjournals.annualreviews.org/errata/anchem.